RSC Advances

PAPER

View Article Online
View Journal | View Issue

Cite this: *RSC Adv.*, 2023, **13**, 34652

Solid polymer electrolytes reinforced with porous polypropylene separators for all-solid-state supercapacitors†

Weidong Liu,[ab] Zhiyun Li,[ab] Fang Pan,[ab] Qingyi He[c] and Qiushi Zhang *[ab]

Solid polymer electrolytes (SPEs) encounter the challenge of balancing high ionic conductivity and mechanical strength. Ionic liquids, which are among the contenders to be used in high-performance supercapacitors, have difficulty infiltrating commercial polyolefin separators for combined applications. In this study, a novel SPE involving uniform infiltration in the micropores of commercial polyolefin separators with polyethylene oxide (PEO), lithium salt, and different proportions of added ionic liquid was developed. The composite membranes combining ionic liquid-filled SPE with polypropylene (PP) microporous separators simultaneously achieve excellent mechanical strength and high-ionic conductivity. The low wettability of pure ionic liquids and commercial polyolefin-based separators is addressed. The 70 wt% IL-filled solid electrolyte composite membrane (PLI(70)@PP) exhibits a high ionic conductivity (2.9 × 10^{-3} S cm^{-1}), low resistance at the electrolyte–electrode interface and excellent mechanical strength (128 MPa) at 25 °C. The all-solid-state supercapacitor using PLI(70)@PP exhibits a specific capacitance of 158 F g^{-1} at 0.1 A g^{-1} and stable cycle performance. The proposed method can be performed *via* high-volume roll-to-roll processing to obtain high-performance all-solid-state supercapacitors (ASSCs) for engineering applications.

Received 29th August 2023
Accepted 21st November 2023

DOI: 10.1039/d3ra05899a

rsc.li/rsc-advances

Introduction

The increasing demand for sustainability and carbon neutrality necessitates new technologies for efficient energy usage and storage. All-solid-state supercapacitors (ASSCs) are novel energy storage devices that feature fast charge–discharge capability and excellent cycle performance. They have garnered considerable attention in recent years. Solid polymer electrolytes (SPEs) are integral components of ASSCs. Unlike traditional liquid electrolytes, SPEs do not pose risks such as flammability, leakage, toxicity, and corrosivity.[1–3] However, the need for high-ionic conductivity and excellent mechanical properties makes SPEs a relevant research subject in the industrial application of ASSCs.[4–8]

Polyethylene oxide (PEO) is a commonly used material in SPEs owing to its low weight, excellent flexibility, and good interfacial compatibility. It is highly porous and provides channels for ionic transport, thus enabling salt ions to fill the pores.[9] However, the narrow electrochemical stability window and low-mechanical strength of PEO limit its application. Thus, scholars have focused on improving the performance of PEO-based SPEs by modifying using inorganic nanoparticles and salts. These modifications have advantages and disadvantages. Inorganic nanoparticles have the potential to enhance both the activity of polymeric chains and ionic conductivity of electrolytes. Nevertheless, their incorporation reduces the mechanical strength of the polymer.[10–12] By contrast, salts can improve the mechanical strength and interfacial stability of electrodes;[13–17] however, ensuring uniform salt dispersion could be considered after commercialization.[18–22] Other techniques, such as electrostatic spinning,[23] hydrogel aerogel,[24] hydrogel,[25] three-dimensional printing,[26] and templates,[27] have been reported to enhance the ionic conductivity of SPEs. Regardless of the method of modification, a primary objective is to simplify the preparation process, which contributes to the further scaling-up and application of solid-state electrolytes.

The separation and insulation properties of conventional SPE membranes fail when temperatures exceed the crystallization melting temperature of the membranes. Equipment without mechanical separators require strict temperature limits, and accidental overheating is a serious safety concern when evaluating equipment performance.[3] This study investigates the reinforcement of commercial separators to achieve stability even at high temperatures.

[a]*College of Automotive Engineering, Jilin University, Changchun 130025, China. E-mail: wdliu@jlu.edu.cn; lizhiyun@jlu.edu.cn; panfang20@mails.jlu.edu.cn; qszhang@jlu.edu.cn; Tel: +86 15843102088*

[b]*State Key Laboratory of Automotive Simulation and Control, Jilin University, Changchun 130012, China*

[c]*Feynman Technology (Qingdao) Co., Ltd., Qingdao 266000, China. E-mail: heqingyi1989@126.com*

† Electronic supplementary information (ESI) available. See DOI: https://doi.org/10.1039/d3ra05899a

Ionic liquids are organic salts and an ideal choice for reinforcing the separator owing to their stable electrochemical properties at high temperatures.[28–30] Ionic liquids exist as liquid compounds at room temperature and comprise organic cations and inorganic/organic anions. These substances demonstrate remarkable stability both chemically and electrochemically, possess negligible vapor pressure, and exhibit high ionic conductivity. Furthermore, ionic liquids are non-inflammable. However, microporous separators typically used in commercial energy storage devices are polyolefin-based materials, such as polypropylene (PP) or polyethylene (PE). The existing commercial polyolefin separators are unsuitable for ionic liquids owing to their hydrophobicity, poor infiltration, and low wettability.[31–34]

In this study, we developed a composite SPE (recorded as PLI(x)@PP) by using a commercial PP separator as the internal reinforcement skeleton of the SPE. The porous PP separator is permeated and encapsulated by the PEO-based SPE (recorded as PLI(x)) in the composite electrolyte, which improves mechanical strength and thermal stability, and the PEO matrix is used as a carrier for adsorbed ions, which solves the low compatibility of commercial polyolefin membranes' with ionic liquids. Ionic liquids establish pathways resembling ion channels *via* strong bonding interactions with the polymer chains of PEO,[35] thereby enhancing the ion conductivity of PLI(x)@PP. The ionic conductivity is increased to fulfil the actual application requirements by changing the ionic liquid content in the PLI(x). The soft PLI(x) on the surface of PP increases the contact area with the electrode and aids in lowering the electrode–electrolyte interface resistance. The electrical performance of the assembled supercapacitor is excellent. This work presents the development of a simple, low-energy PLI(x)@PP, which has the potential to employ large-scale roll-to-roll production.

Materials and methods

Materials

The compounds used were as follows: PEO (Mw = 600 000, Sigma), lithium bis(trifluoromethane sulfonyl)imide (LiTFSI) (99.95%, Sigma), ionic liquid 1-ethyl-3-methylimidazolium tetrafluoroborate (IL) (≥99.0%, Sigma), polypropylene separator (single-layer PP separator, Zhongxing Innovative Material Technologies Co., Ltd.), carbon electrode (AC, YP-50F, Kuraray, Japan), carbon black (CB, EC 600 J, Ketjen Black, Japan), polyvinylidene fluoride (PVDF, 99.5%, Hefei Kejing Material Technology), *N*-methyl-pyrrolidone (>99.0%, Aladdin Chemical Reagent), and acetone (>99.0%, Aladdin Chemical Reagent).

Preparation of PLI(x) solid electrolyte membrane

Half a gram of PEO and 0.18 g LiTFSI were dissolved in acetone (10 mL) and stirred at 50 °C to obtain a homogeneous solution (PEO : Li = 18 : 1, molar ratio). Subsequently, different proportions of IL (0%, 20%, 33%, 40%, 50%, 60%, and 70% of the total mass of PEO-LiTFSI-IL) were separately added to the solution and stirred vigorously for 12 h at 50 °C to prepare a series of solution samples. The solution was poured onto polytetrafluoroethylene (PTFE) moulds and smoothened with a squeegee after defoaming. The membrane (PLI(x)) was vacuum-dried at 40 °C for 24 h. Finally, a thin layer of release agent was applied to the PTFE moulds to prevent sticking.

PLI(x)@PP membrane preparation

The same procedure as that with the PLI(x) membrane preparation was followed to prepare PLI(x)@PP (x = 0, 20, 33, 40, 50, 60, 70) membranes, except that the PLI(x) solution was poured onto both sides of the PP separator, which was laid flat on the PTFE mould. The specimen was then vacuum-dried in an oven at 40 °C for 24 h to remove the solvent.

Electrode preparation

The electrode solution was prepared by mixing AC, CB, and PVDF powders (mass ratio of 8 : 1 : 1) with *N*-methyl pyrrolidone *via* vigorous magnetic stirring overnight. The homogeneous mixture was then coated on aluminium foil and transferred into a 100 °C oven for 12 h to obtain the carbon electrode (CE). The electrode was perforated into a disk (diameter = 13 mm).

Electrochemical testing

Electrochemical impedance spectroscopy (EIS) and cyclic voltammetry (CV) were performed using an electrochemical workstation (CHI660E, Shanghai Chenhua Device Company, China). The CV test conditions included a voltage of 0–2.5 V potential range and a scan rate in the 10–100 mV s^{-1} range. Sample films for EIS were sandwiched between two stainless sheets, and data were collected under conditions with a 5 mV amplitude and a 10^{-1}–10^{6} Hz frequency range. EIS could be used to determine the equivalent series resistance (ESR) and charge transfer resistance of the film device. The samples were placed in an environmentally controlled chamber for high-temperature tests (25–70 °C). The temperature for each test was maintained for 30 min to ensure stability. The ionic conductivity was calculated from the EIS spectra using the following equation.

$$\delta = \frac{L}{R_s \times S}, \quad (1)$$

where L, S, and R_s denote the thickness, area, and bulk resistance of the PLI(x)@PP membranes, respectively (R_s corresponds to the x-axis intercept of the impedance response).

The ASSC galvanostatic charge–discharge (GCD) cycle was completed using the blue battery test System (CT2001A, Land Electronic). The voltage range was 0–2.5 V, and different current densities (ratio of current to the mass of a single electrode) were measured. The capacitance of ASSCs (C_{cell}, F) was calculated from the discharge curve of GCD. The specific capacitance of electrode (C_{sp}, F g^{-1}), energy density (E, Wh kg^{-1}), and power density (P, W kg^{-1}) of ASSCs were calculated using the following equations.[36–38]

$$C_{cell} = \frac{I \times \Delta t}{\Delta V} \quad (2)$$

$$C_{sp} = \frac{2C_{cell}}{m} \quad (3)$$

$$E = \frac{C_{cell} \times (\Delta V)^2}{4m \times 3.6} \quad (4)$$

$$P = \frac{E}{\Delta t} \times 3600, \quad (5)$$

where I denotes the discharge current (A), Δt indicates the discharge time (s), ΔV refers to the voltage value (V) during discharge after the voltage jump/drop (IR), and m denotes the AC mass (g) for one electrode.

Thermal performance testing

A differential scanning calorimeter (DSC, model HSC-4, Beijing permanent laboratory equipment Co., Ltd) was used to detect the melting temperature (T_m) and melting enthalpy (ΔH) of the electrolytes. The temperature range and heating rate were 0–100 °C and 10 °C min^{-1}, respectively. T_m denotes the minimum heat absorption peak caused by the crystalline phase melting. The degree of crystallinity (X_c, %) was calculated as follows:

$$X_c = \frac{\Delta H}{\Delta H_0} \times 100, \quad (6)$$

where ΔH indicates the melting enthalpy (J g^{-1}) expressed as heat absorbed per unit weight of the polymer sample, and ΔH_0 denotes the melting enthalpy of 100% crystalline PEO (213.7 J g^{-1}).[39]

Material characterization

The membrane morphology was characterized using a field emission scanning electron microscope (SEM, xl30esem-FEG, FEI). Cross-sectional elemental analysis was performed using X-ray energy dispersive spectrometry (EDS). The edges of the dried PLI(x)@PP membranes were notched, immersed in liquid nitrogen, and torn off to obtain test samples with unmetallized cross-sections.

A tensile test was performed using a GOTECH AI-7000SUT tensile machine at 25 °C according to the ASTM D882 standard, with a film size, fixture spacing, and tensile rate of 150 mm × 12 mm, 100 mm, and 50 mm min^{-1}, respectively. The tensile strength and toughness were averaged over five samples.

Results and discussion

In this study, a novel solid polymer electrolyte composite membrane was prepared by thoroughly permeating PP separators with a PLI(x) electrolyte solution (Fig. 1). This method is distinct from the conventional dispersed mixing of polymers and inorganic nanoparticles. The PEO matrix of the developed PLI(x)@PP membrane provided a channel for ions in separator pores. Additionally, the PP separators served as a structural backbone to provide strength. These two characteristics addressed the problems of incompatibility between IL and PP (Fig. S1†), as well as the poor mechanical strength of the PEO matrix. The proposed preparation method also enables the application of a roll-to-roll process and product-scale production, making it suitable for numerous potential applications.

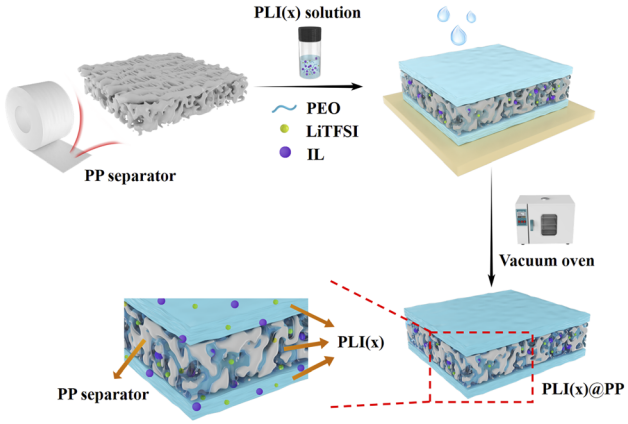

Fig. 1 Schematic of PLI(x)@PP preparation.

Optical photographs of membranes with different proportions of IL show that the membrane transparency gradually increased with the addition of the IL (Fig. 2a). This phenomenon was caused by the photorefraction as the light penetrated the micropores, suggesting that more IL was present in the PP separators.

SEM imaging revealed micron-sized pores on the surfaces of the PP separators (Fig. 2b); these pores facilitated the PLI(x) solution penetration. Additionally, the smooth surfaces of PP separators indicated that PLI(x) was also uniformly coated on the surface of PP (Fig. 2c–i). Moreover, the membrane surface exhibited a folded morphology as IL increased in the PLI(x); this change was caused by the capillary force after PLI(x) penetrated the PP micropores.[40]

The PP separator in the PLI(40)@PP cross-section was approximately 16 μm thick; soft PLI(x) electrolyte layers (II and IV) on both surfaces of the separator with a thickness of approximately 5 μm (Fig. 2j) were observed. The distributions

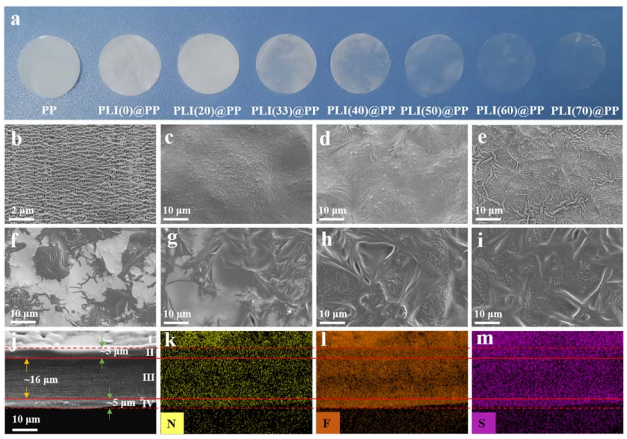

Fig. 2 (a) Optical photographs of PP separators and PLI(0)@PP-PLI(70)@PP membranes, (b–i) SEM images of PP and PLI(x)@PP surface, (j) SEM images of the PLI(40)@PP membrane cross-section, and (k–m) corresponding EDS elemental maps of N, F, and S.

of N, F, and S in this cross-section showed that the PLI(x) electrolyte was uniformly dispersed on the surfaces of PLI(40)@PP(I), internal PP separator (III), and the PLI(x) layers (II and IV) (Fig. 2k–m). The element distributions inside the separator were slightly sparser because the PLI(x) electrolyte only infiltrated the separator pores (Fig. S3†).

In addition, the gradually decreased element sulphur (S) (specific to LiTFSI) in the cross-section (Fig. S2†) indicates that the percentage of LiTFSI decreased. This change was caused by the gradual rise in IL, indirectly explaining the variation in the optical photographs of the PLI(x)@PP membranes described previously.

An evaluation of the PLI(x) electrolyte thermal properties revealed a relatively sharp peak of heat absorption at 70.9 °C for pure PEO (Fig. 3a). The melting peak and peak width shifted towards lower temperatures with the addition of LiTFSI and different IL concentrations to the PEO matrix (Table S1†). A lower T_m is expected following the addition of salt to the polymer and has been associated with a decreased spherical crystal size and surface free energy.[41,42] The ΔH of crystallization indicates the melting peak area (proportional to X_c) of the DSC curve. Reductions in T_m and ΔH with the addition of salt indicate a lower crystallinity and elevation of the amorphous region in PEO.[43] Moreover, the segmental motion of the PEO molecules and ion transport were both enhanced owing to the higher flexibility and fluidity of amorphous PEO chains.

As shown in Fig. 3b, mechanical tensile tests were conducted on the PP, PLI(x)@PP, and PLI(0) membranes. The maximum tensile strength for all three membranes was approximately 128 MPa, and the fracture elongation increased with the IL content. Compared to the PP separator, the fracture strength of the PLI(x)@PP membrane was slightly lower, but it exhibited better toughness. This tendency can be attributed to the infiltration of the soft PLI electrolyte into the micro-pores of the PP separator, which enhanced the plasticity of the PP separator matrix. Furthermore, the PLI(0) sample without a PP separator as a reference showed a fracture strength of only 1.8 MPa but a fracture elongation as high as 1100%. This result indicates that the presence of the PP separator significantly improved the strength of the electrolyte membrane.

In addition to the mechanical tests, the Nyquist plot of the PLI(x)@PP membranes is illustrated in Fig. 3c. A semicircular characteristic exists in the high-frequency region, and a linear characteristic can be observed in the low-frequency region, indicating a standard double-layer capacitance behaviour. In the region of high frequency, the curve intersects the x-axis at a decreasing rate, and the diameter of the semicircle shifts towards the high-frequency area. This observation suggests that a higher IL content is efficient for diminishing the ESR and charge transfer resistance. In the low-frequency region, the linear slope, which represents the rate of charge diffusion, steepens with the increasing IL content, indicating that the charge diffuses faster in electrolytes with high IL content. The Nyquist diagram simulated by the equivalent circuit diagram is shown in Fig. 3d. R_s and R_f represent the ESR and charge transfer resistance, respectively. W1 represents the charge diffusion impedance, and the curve plotted in Fig. 3d shows the trend of decreasing ESR and charge transfer resistance with increasing IL content in PLI(x)@PP. As shown in Fig. 3e, the corresponding ionic conductivities of the PLI(x)@PP membranes are 9.6×10^{-6}, 3.4×10^{-5}, 5.1×10^{-5}, 1.2×10^{-4}, 4.7×10^{-4}, 1.7×10^{-3}, and 2.9×10^{-3} S cm^{-1}. The positive correlation between the ionic conductivity and IL concentration may have been caused by the increase in the charge carrier density; IL enhances lithium salt dissociation and polymer segmental motion by weakening chain forces.[44–46] Furthermore, the ionic conductivity of the PLI(x)@PP membranes exhibit a strong temperature dependence (Fig. 3f); the ionic conductivity of the PLI(x)@PP membranes increased as temperatures increased within the range of 25–70 °C. The elevated ion mobility and chain segmentation at 70 °C resulted in an ionic conductivity of nearly 10^{-2} S cm^{-1} for PLI(70)@PP, which is comparable with the highest reported values.[47]

CE/PLI(x)@PP/CEs were assembled using two carbon electrodes and a PLI(x)@PP membrane. We performed cyclic voltammetry (CV) tests on the assembled CE/PLI(x)@PP/CEs, as shown in Fig. 4a. As the IL content increased, the CV curve area expanded, indicating an increase in the capacitance of the device. Charge–discharge cycles of the CE/PLI(x)@PP/CEs were performed at 25 °C (Fig. 4b). The area under the galvanostatic charge–discharge (GCD) curves increased with the IL content. This finding indicates that the specific capacitance of CE/

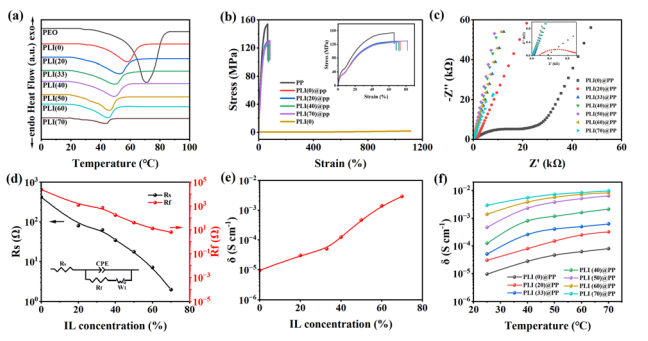

Fig. 3 (a) DSC curves of PEO and PLI(x), (b) stress–strain curves of the composite membrane PLI(x)@PP and the pure electrolyte membrane PLI(0), (c) impedance spectrogram test results (25 °C), (d) reduction in ESR (R_s) and charge transfer resistance (R_f) with increasing IL content in PLI(x)@PP, (e) ionic conductivity at 25 °C, and (f) ionic conductivity trends across a range of temperatures (25–70 °C).

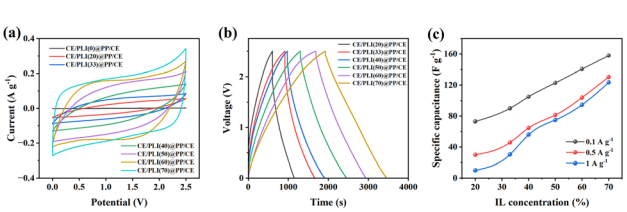

Fig. 4 (a) CV curves of CE/PLI(x)@PP/CE assemblies with different PLI(x)@PP compositions, (b) GCD curves of CE/PLI(x)@PP/CE at 0.1 A g^{-1}, and (c) specific capacitance of CE/PLI(x)@PP/CE at different current densities.

PLI(70)@PP/CE is the highest among all samples (Fig. 4c) at 70 wt% of the IL. Moreover, the voltage IR decreased as IL increased, indicating the lower equivalent series resistance (ESR) of this specific ASSC. This characteristic can be attributed to the softer electrolyte layer, which lowered the interface resistance of the electrode, and it is consistent with ionic conductivity results.

The CV curves for the CE/PLI(70)@PP/CE were estimated at different scan rates and room temperature (Fig. 5a). At low-scan rates, the CV curves were rectangular; however, deviations from that shape occurred at high scan rates for ideal double-layer capacitors, possibly because of resistance and overpotential.[48]

However, CV could not fully explain the electrochemical properties of the CE/PLI(70)@PP/CE. Therefore, the GCD measurements were performed at various current densities (Fig. 5b). The charge–discharge curves exhibit triangular linear profiles, typical of double-layer capacitors. The results confirm their superior capacitive properties. The charge–discharge curves of the CE/PLI(70)@PP/CE at various current densities reveal that the area under the GCD curves decreased as the current density increased. The specific capacitance of the CE/PLI(70)@PP/CE increased to 158 F g^{-1} at 0.1 A g^{-1} (Fig. 5c), a value at the higher end of reported values among polymer electrolytes mixed with IL (Table S2†). The CE/PLI(70)@PP/CE demonstrated a high-energy density of 32.1 Wh kg^{-1} and power density of 75.6 W kg^{-1} with a current density of 0.1 A g^{-1}; the energy and power densities were low at 13.8 Wh kg^{-1} and 1.06 kW kg^{-1} (Fig. 5c), respectively, with a current density of 1 A g^{-1}. The developed membranes exhibit excellent energy and power densities compared with those reported in the literature (Fig. S4†) and outperformed similar supercapacitors in terms of the energy density.[49,50] A red light-emitting diode (LED) (2 V) could be lit for a few minutes after charging the ASSC to 2.5 V (Fig. 5c).

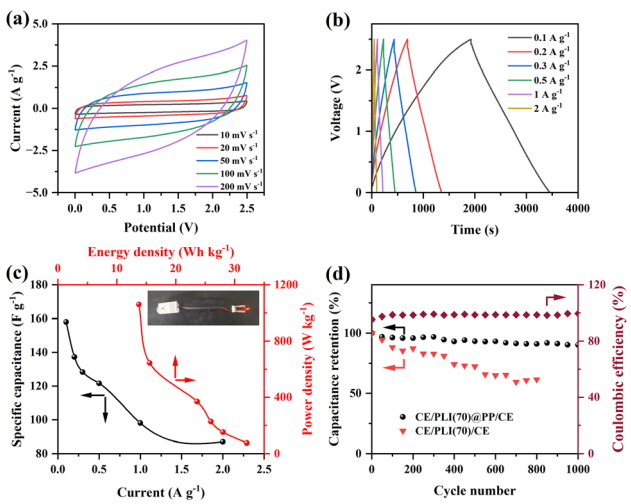

Fig. 5 Electrochemical results for (CE)/PLI(70)@PP/CE: (a) CV curves at different current densities, (b) GCD curves at different current densities, (c) current density plots against specific capacity and energy density against power density, and (d) capacitance retention and coulombic efficiency across 1000 cycles.

One thousand charge–discharge cycles of the CE/PLI(70)@PP/CE were performed at a current density of 1 A g^{-1} (Fig. S5†). The charge–discharge cycle curves of the quasi-isosceles triangle yielded a minimal increase in the IR after 1000 cycles, thus indicating charge transport stability between the electrode and electrolyte interfaces.[51] The discharge capacity of the CE/PLI(70)@PP/CE gradually decreased with the number of cycles (Fig. 5d). Its capacity retention after 1000 cycles reached 90% of the initial capacity. The coulombic efficiency was high (99.37%) over 1000 cycles, demonstrating the excellent cycle stability of the device. By contrast, the capacity retention of the CE/PLI(70)/CE ASSC decreased considerably with cycling, reaching values as low as 60% after 800 cycles. The difference in the cycle stability of ACCSs was revealed by comparing the semicircular diameter change of the EIS curve before and after cycling. The CE/PLI(70)@PP/CE exhibited lower R_f and range of variation after cycling than CE/PLI(70)/CE (Fig. S6a†). After CE/PLI(70)@PP/CE cycling, a slight increase in Rf (semicircular EIS diameter) was associated with a decrease in IL content within PLI(70)@PP (reduced F-element content in the EDS spectrum, Fig. S6b†). The porous PP separator with network structure can hinder the local chain reorganization of the polymer electrolyte owing to its large surface area. This leads to the presence of highly amorphous regions in the polymeric matrix, favouring ionic migration.[52] These results indicate that the PP separator provides a more stable support structure and ionic transport channel.

Thermal stability tests were conducted on the PLI(x) and PLI(x)@PP membranes (Fig. S7†). All membranes show dimensional stability at temperatures below 40 °C. The PLI(70) membrane without the PP separator as the backbone melted into a viscous liquid at 50 °C, whereas the PLI(70)@PP membrane remained intact even at 70 °C. Additionally, no IL exudation was observed on the PLI(70)@PP membrane, indicating its stable morphology at high temperatures. This phenomenon suggests that the PP separator functions as a structural backbone, ensuring the morphological stability of the composite membrane at high temperatures, which forms the basis for maintaining stable electrical properties.

The mechanical and electrical performance of PLI(70)@PP were characterized at various temperatures (25–70 °C). Fig. 6a presents the mechanical performance of the PLI(70)@PP membrane at different temperatures, exhibiting a decrease in mechanical performance (Fig. S8†) and an increase in elongation at higher temperatures. This finding can be attributed to the elevated temperatures causing increased movement of the PP molecular chains, which dominates the mechanical performance.

Furthermore, concerning the electrical properties, Fig. 6b illustrates the EIS curves at various temperatures. In the high-frequency range, the curves demonstrate a decrease in the intercept with the *x*-axis, whereas the slope increases in the low-frequency range. This characteristic suggests that higher temperatures can reduce the equivalent series resistance and charge transfer resistance of the device, potentially owing to enhanced interface compatibility between the electrode and electrolyte as the temperature increases.

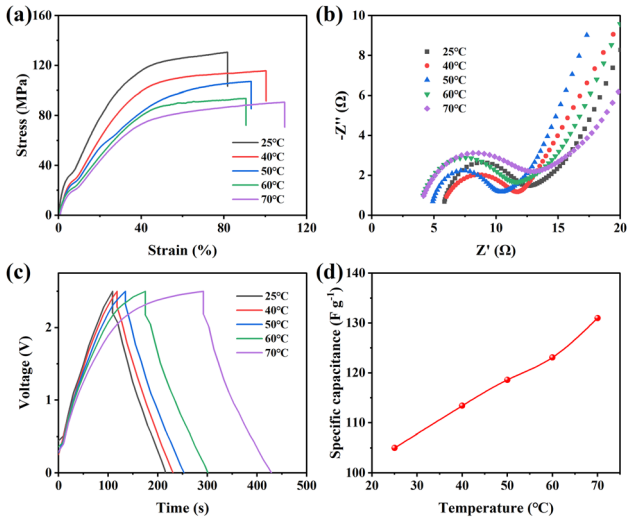

Fig. 6 Mechanical and electrochemical properties of PLI(70)@PP at 25–70 °C. (a) Stress–strain curve; (b) EIS impedance spectrum; (c) GCD curve; (d) specific capacitance calculated from the GCD measurements.

The GCD curves for CE/PLI(70)@PP/CE, with a current density of 1 A g^{-1}, were measured at different temperatures (25–70 °C), as depicted in Fig. 6c. The CE/PLI(70)@PP/CE electrode exhibits an increase in specific capacity during charge–discharge cycles at higher temperatures, as observed in Fig. 6d. This increase is likely to have resulted from the improved migration of PLI(70) into the AC electrode pores at elevated temperatures, resulting in the increased contact area between the electrolyte and electrode.[53]

Conclusions

In this study, a composite SPE was developed using a PP membrane reinforcement. The PLI(70)@PP membrane exhibited a high ionic conductivity of 2.9 × 10^{-3} S cm^{-1} at 25 °C, along with low electrolyte–electrode interface resistance and excellent mechanical properties. The CE/PLI(70)@PP/CE devices, with a specific capacity of 158 F g^{-1}, demonstrated superior energy and power densities as well as stable cycling performance. The PLI(70)@PP maintained a stable mechanical structure and showed excellent electrochemical performance at 25–70 °C. This work presents a facile and effective composite solid polymer electrolyte (PLI(x)@PP), which shows potential for large-scale roll-to-roll preparation processes and is considered a solid electrolyte candidate for the development of high-performance ASSCs.

Author contributions

Weidong Liu: conceptualization, validation, funding acquisition, supervision, writing – review & editing, project administration. Zhiyun Li: methodology, investigation, writing – original draft, visualization, writing – review & editing. Fang Pan: investigation, resources, writing – original draft, writing – review & editing. Qingyi He: conceptualization, investigation, resources, project administration. Qiushi Zhang: conceptualization, writing – review & editing, supervision, project administration.

Conflicts of interest

There are no conflicts to declare.

Acknowledgements

The research was supported by the State Key Laboratory of Automotive Simulation and Control (ASCL) and the Frontier Materials and High-end Equipment Expert Workstation of Qingdao. We would like to thank Jifu Zheng from the Key Laboratory of Polymer Ecomaterials, Changchun Institute of Applied Chemistry, Chinese Academy of Sciences, for the SEM analysis.

Notes and references

1 H. Gao and K. Lian, Proton-conducting polymer electrolytes and their applications in solid supercapacitors: a review, *RSC Adv.*, 2014, **4**, 33091–33113.
2 S. A. Alexandre, G. G. Silva, R. Santamaría, J. P. C. Trigueiro and R. L. Lavall, A highly adhesive PIL/IL gel polymer electrolyte for use in flexible solid-state supercapacitors, *Electrochim. Acta*, 2019, **299**, 789–799.
3 X. Zhang, M. Kar, T. C. Mendes, Y. Wu and D. R. MacFarlane, Supported ionic liquid gel membrane electrolytes for flexible supercapacitors, *Adv. Energy Mater.*, 2018, **8**, 1702702.
4 Z.-S. Wu, X. Feng and H.-M. Cheng, Recent advances in graphene-based planar micro-supercapacitors for on-chip energy storage, *Natl. Sci. Rev.*, 2014, **1**, 277–292.
5 H. Gao and K. Lian, Advanced proton conducting membrane for ultra-high rate solid flexible electrochemical capacitors, *J. Mater. Chem.*, 2012, **22**, 21272–21278.
6 H. Gao, A. Virya and K. Lian, Proton conducting H5BW12O40 electrolyte for solid supercapacitors, *J. Mater. Chem. A*, 2015, **3**, 21511–21517.
7 Y. J. Kang, Y. Yoo and W. Kim, 3-V Solid-State Flexible Supercapacitors with Ionic-Liquid-Based Polymer Gel Electrolyte for AC Line Filtering, *ACS Appl. Mater. Interfaces*, 2016, **8**, 13909–13917.
8 S. Pilathottathil, T. K. Kottummal, M. S. Thayyil, P. Mahadevan Perumal and J. A. Purakakath, Inorganic salt grafted ionic liquid gel electrolytes for efficient solid state supercapacitors: Electrochemical and dielectric studies, *J. Mol. Liq.*, 2018, **264**, 72–79.
9 G. Chen, Y. Bai, Y. Gao, Z. Wang, K. Zhang, Q. Ni, F. Wu, H. Xu and C. Wu, Inhibition of crystallization of poly (ethylene oxide) by ionic liquid: insight into plasticizing mechanism and application for solid-state sodium ion batteries, *ACS Appl. Mater. Interfaces*, 2019, **11**, 43252–43260.
10 D. F. Miranda, C. Versek, M. T. Tuominen, T. P. Russell and J. J. Watkins, Cross-Linked Block Copolymer/Ionic Liquid Self-Assembled Blends for Polymer Gel Electrolytes with

High Ionic Conductivity and Mechanical Strength, *Macromolecules*, 2013, **46**, 9313–9323.

11 H. Wang, C. Lin, X. Yan, A. Wu, S. Shen, G. Wei and J. Zhang, Mechanical property-reinforced PEO/PVDF/LiClO4/SN blend all solid polymer electrolyte for lithium ion batteries, *J. Electroanal. Chem.*, 2020, **869**, 114156.

12 J. Mindemark, M. J. Lacey, T. Bowden and D. Brandell, Beyond PEO-Alternative host materials for Li+-conducting solid polymer electrolytes, *Prog. Polym. Sci.*, 2018, **81**, 114–143.

13 O. Geiculescu, J. Yang, S. Zhou, G. Shafer, Y. Xie, J. Albright, S. Creager, W. Pennington and D. DesMarteau, Solid polymer electrolytes from polyanionic lithium salts based on the LiTFSI anion structure, *J. Electrochem. Soc.*, 2004, **151**, A1363.

14 M. Marzantowicz, J. R. Dygas, F. Krok, J. L. Nowiński, A. Tomaszewska, Z. Florjańczyk and E. Zygadło-Monikowska, Crystalline phases, morphology and conductivity of PEO:LiTFSI electrolytes in the eutectic region, *J. Power Sources*, 2006, **159**, 420–430.

15 L. Li, Y. Deng and G. Chen, Status and prospect of garnet/polymer solid composite electrolytes for all-solid-state lithium batteries, *J. Energy Chem.*, 2020, **50**, 154–177.

16 S. Wang, Q. Zeng, A. Wang, X. Liu, J. Chen, Z. Wang and L. Zhang, Constructing stable ordered ion channels for a solid electrolyte membrane with high ionic conductivity by combining the advantages of liquid crystal and ionic liquid, *J. Mater. Chem. A*, 2019, **7**, 1069–1075.

17 S. Cheng, D. M. Smith and C. Y. Li, How Does Nanoscale Crystalline Structure Affect Ion Transport in Solid Polymer Electrolytes?, *Macromolecules*, 2014, **47**, 3978–3986.

18 Y.-J. Lim, Y.-H. An and N.-J. Jo, Polystyrene-Al2O3 composite solid polymer electrolyte for lithium secondary battery, *Nanoscale Res. Lett.*, 2012, **7**, 19.

19 S. A. Suthanthiraraj and D. J. Sheeba, Structural investigation on PEO-based polymer electrolytes dispersed with Al2O3 nanoparticles, *Ionics*, 2007, **13**, 447–450.

20 H.-M. Xiong, Z.-D. Wang, D.-P. Xie, L. Cheng and Y.-Y. Xia, Stable polymer electrolytes based on polyether-grafted ZnO nanoparticles for all-solid-state lithium batteries, *J. Mater. Chem.*, 2006, **16**, 1345–1349.

21 N. Zhang, J. He, W. Han and Y. Wang, Composite solid electrolyte PEO/SN/LiAlO2 for a solid-state lithium battery, *J. Mater. Sci.*, 2019, **54**, 9603–9612.

22 J. Li, K. Zhu, Z. Yao, G. Qian, J. Zhang, K. Yan and J. Wang, A promising composite solid electrolyte incorporating LLZO into PEO/PVDF matrix for all-solid-state lithium-ion batteries, *Ionics*, 2020, **26**, 1101–1108.

23 D. Li, L. Chen, T. Wang and L.-Z. Fan, 3D Fiber-Network-Reinforced Bicontinuous Composite Solid Electrolyte for Dendrite-free Lithium Metal Batteries, *ACS Appl. Mater. Interfaces*, 2018, **10**, 7069–7078.

24 W. Jia, Z. Li, Z. Wu, L. Wang, B. Wu, Y. Wang, Y. Cao and J. Li, Graphene oxide as a filler to improve the performance of PAN-LiClO4 flexible solid polymer electrolyte, *Solid State Ionics*, 2018, **315**, 7–13.

25 J. Bae, Y. Li, J. Zhang, X. Zhou, F. Zhao, Y. Shi, J. B. Goodenough and G. Yu, A 3D nanostructured hydrogel-framework-derived high-performance composite polymer lithium-ion electrolyte, *Angew. Chem., Int. Ed.*, 2018, **57**, 2096–2100.

26 S. Zekoll, C. Marriner-Edwards, A. K. O. Hekselman, J. Kasemchainan, C. Kuss, D. E. J. Armstrong, D. Cai, R. J. Wallace, F. H. Richter, J. H. J. Thijssen and P. G. Bruce, Hybrid electrolytes with 3D bicontinuous ordered ceramic and polymer microchannels for all-solid-state batteries, *Energy Environ. Sci.*, 2018, **11**, 185–201.

27 K. K. Fu, Y. Gong, G. T. Hitz, D. W. McOwen, Y. Li, S. Xu, Y. Wen, L. Zhang, C. Wang and G. Pastel, Three-dimensional bilayer garnet solid electrolyte based high energy density lithium metal–sulfur batteries, *Energy Environ. Sci.*, 2017, **10**, 1568–1575.

28 A. Ray and B. Saruhan, Application of ionic liquids for batteries and supercapacitors, *Materials*, 2021, **14**, 2942.

29 Q. Yang, Z. Zhang, X.-G. Sun, Y.-S. Hu, H. Xing and S. Dai, Ionic liquids and derived materials for lithium and sodium batteries, *Chem. Soc. Rev.*, 2018, **47**, 2020–2064.

30 A. Eftekhari, Supercapacitors utilising ionic liquids, *Energy Stor. Mater.*, 2017, **9**, 47–69.

31 Y. Song, L. Sheng, L. Wang, H. Xu and X. He, From separator to membrane: Separators can function more in lithium ion batteries, *Electrochem. Commun.*, 2021, **124**, 106948.

32 C. S. Stefan, D. Lemordant, B. Claude-Montigny and D. Violleau, Are ionic liquids based on pyrrolidinium imide able to wet separators and electrodes used for Li-ion batteries?, *J. Power Sources*, 2009, **189**, 1174–1178.

33 M. M. Huie, R. A. DiLeo, A. C. Marschilok, K. J. Takeuchi and E. S. Takeuchi, Ionic liquid hybrid electrolytes for lithium-ion batteries: a key role of the separator–electrolyte interface in battery electrochemistry, *ACS Appl. Mater. Interfaces*, 2015, **7**, 11724–11731.

34 M. Kirchhöfer, J. Von Zamory, E. Paillard and S. Passerini, Separators for Li-ion and Li-Metal battery including ionic liquid based electrolytes based on the TFSI− and FSI− anions, *Int. J. Mol. Sci.*, 2014, **15**, 14868–14890.

35 J. H. Lee, J. S. Chae, J. H. Jeong, *et al.*, Ionic liquid incorporated in quasi-solid-state electrolyte for high-temperature supercapacitor applications, *Chem. Commun.*, 2019, **55**, 15081–15084.

36 R. Muchakayala, S. Song, J. Wang, Y. Fan, M. Bengeppagari, J. Chen and M. Tan, Development and supercapacitor application of ionic liquid-incorporated gel polymer electrolyte films, *J. Ind. Eng. Chem.*, 2018, **59**, 79–89.

37 S. Zhang and N. Pan, Supercapacitors performance evaluation, *Adv. Energy Mater.*, 2015, **5**, 1401401.

38 J. Xie, P. Yang, Y. Wang, T. Qi, Y. Lei and C. M. Li, Puzzles and confusions in supercapacitor and battery: Theory and solutions, *J. Power Sources*, 2018, **401**, 213–223.

39 J. Shin, K. Kim, H. Ahn and J. Ahn, Electrochemical properties and interfacial stability of (PEO) 10LiCF3SO3–TinO2n− 1 composite polymer electrolytes for lithium/sulfur battery, *Mater. Sci. Eng. B*, 2002, **95**, 148–156.

40 X. Yang, Q. Sun, C. Zhao, X. Gao, K. R. Adair, Y. Liu, J. Luo, X. Lin, J. Liang and H. Huang, High-areal-capacity all-solid-state lithium batteries enabled by rational design of fast ion transport channels in vertically-aligned composite polymer electrodes, *Nano Energy*, 2019, **61**, 567–575.

41 R. Nadimicherla, A. Sharma, V. Rao and W. Chen, Electrical and solid-state battery performance of a new PVC/PEO+ KBr blend-based polymer electrolyte system, *Ionics*, 2015, **21**, 1587–1594.

42 M. Ravi, S. Song, J. Wang, R. Nadimicherla and Z. Zhang, Preparation and characterization of biodegradable poly (ε-caprolactone)-based gel polymer electrolyte films, *Ionics*, 2016, **22**, 661–670.

43 M. Jacob and A. Arof, FTIR studies of DMF plasticized polyvinyledene fluoride based polymer electrolytes, *Electrochim. Acta*, 2000, **45**, 1701–1706.

44 S. N. Banitaba, D. Semnani, B. Rezaei and A. A. Ensafi, Evaluating the electrochemical properties of PEO-based nanofibrous electrolytes incorporated with TiO2 nanofiller applicable in lithium-ion batteries, *Polym. Adv. Technol.*, 2019, **30**, 1234–1242.

45 K. Karuppasamy, H. W. Rhee, P. A. Reddy, D. Gupta, L. Mitu, A. R. Polu and X. S. Shajan, Ionic liquid incorporated nanocomposite polymer electrolytes for rechargeable lithium ion battery: A way to achieve improved electrochemical and interfacial properties, *J. Ind. Eng. Chem.*, 2016, **40**, 168–176.

46 R. K. Arya and A. K. Gupta, The effect of nitrogen-rich ionic liquid [EMIMDCA] on the electronic structure of solid polymer electrolyte (PEO-LiTFSI), *J. Mol. Model.*, 2022, **28**, 363.

47 F. González, V. Gregorio, A. Rubio, L. Garrido, N. García and P. Tiemblo, Ionic liquid-based thermoplastic solid electrolytes processed by solvent-free procedures, *Polymers*, 2018, **10**, 124.

48 A. S. Westover, B. Baer, B. H. Bello, H. Sun, L. Oakes, L. M. Bellan and C. L. Pint, Multifunctional high strength and high energy epoxy composite structural supercapacitors with wet-dry operational stability, *J. Mater. Chem. A*, 2015, **3**, 20097–20102.

49 H. Niu, L. Wang, P. Guan, N. Zhang, C. Yan, M. Ding, X. Guo, T. Huang and X. Hu, Recent advances in application of ionic liquids in electrolyte of lithium ion batteries, *J. Energy Storage*, 2021, **40**, 102659.

50 Y. Wang, Y. Song and Y. Xia, Electrochemical capacitors: mechanism, materials, systems, characterization and applications, *Chem. Soc. Rev.*, 2016, **45**, 5925–5950.

51 S. Alipoori, S. Mazinani, S. H. Aboutalebi and F. Sharif, Review of PVA-based gel polymer electrolytes in flexible solid-state supercapacitors: Opportunities and challenges, *J. Energy Storage*, 2020, **27**, 101072.

52 H. Yang and N. Wu, Ionic conductivity and ion transport mechanisms of solid-state lithium-ion battery electrolytes: A review, *Energy Sci. Eng.*, 2022, **10**, 1643–1671.

53 T. Mao, S. Wang, X. Wang, F. Liu, J. Li, H. Chen, D. Wang, G. Liu, J. Xu and Z. Wang, High-temperature and all-solid-state flexible supercapacitors with excellent long-term stability based on porous polybenzimidazole/functional ionic liquid electrolyte, *ACS Appl. Mater. Interfaces*, 2019, **11**, 17742–17750.